Inorganic Chemistry
Cite This: Inorg. Chem. XXXX, XXX, XXX−XXX
Communication
pubs.acs.org/IC

Two-Way Alloying and Dealloying of Cadmium in Metalloid Gold Clusters

Wenhao Zhang,[†,‡,§,⊥] Shengli Zhuang,[†,§,⊥] Lingwen Liao,[†,§] Hongwei Dong,[†,‡,§] Nan Xia,[†,§] Jin Li,[∥] Haiteng Deng,[¶] and Zhikun Wu*[,†,§]

[†]Key Laboratory of Materials Physics, Anhui Key Laboratory of Nanomaterials and Nanotechnology, CAS Center for Excellence in Nanoscience, Institute of Solid State Physics, Chinese Academy of Sciences, Hefei, Anhui 230031, P. R. China

[‡]University of Science and Technology of China, Hefei, Anhui 230026, P. R. China

[§]Institute of Physical Science and Information Technology, Anhui University, Hefei, Anhui 230026, P. R. China

[∥]Tsinghua University-Peking University Joint Center for Life Sciences, School of Life Sciences, and [¶]MOE Key Laboratory of Bioinformatics, School of Life Sciences, Tsinghua University, Beijing 100084, P. R. China

Supporting Information

ABSTRACT: The alloying of monometal nanoparticles with a transition element has recently attracted extensive interest; however, the dealloying of alloy nanoparticles has rarely been reported. Two-way alloying and dealloying in metal nanoparticles is not known so far to the best of our knowledge. In this work, for the first time, we successfully achieved two-way alloying and dealloying of cadmium in metalloid gold clusters via an antigalvanic reaction in combination with a quasi-antigalvanic reaction and demonstrated reactant-ion-dependent dealloying as well.

The alloying of metal nanoparticles is of great significance not only for fundamental scientific research but also for practical applications because alloying can effectively tune the structural and electronic properties of metal nanoparticles.[1] However, for relatively larger metal nanoparticles, conventional characterization techniques, such as electron microscopy, cannot always map an atomically precise structure, especially the surface structure, to the extent that the alloying effects and resultant properties can be understood in-depth.[2] The emergences of metalloid clusters[2−7] with well-defined compositions and structures provide excellent platforms for solving these challenging issues.[8e,9a,b] The majority of previous research on metalloid cluster alloying focused on silver, copper, and gold metals.[8] Recently, metalloid gold clusters alloyed with IIB group metals, such as cadmium (Cd) and mercury,[9] are highly regarded not only because Cd is an active metal compared to the previously mentioned elements but also because Cd alloying leads to rich structures and properties of metalloid gold clusters. For example, three Cd alloying modes have been observed to date. The first case is that the Cd atom replaces a kernel atom in the metalloid gold cluster 1:1 without altering the staple structure, such as in $Au_{24}Cd(CH_2CH_2Ph)_{18}$.[9c] The second case is that the Cd atoms occupy both the kernel and staple positions of the metalloid gold clusters, changing the original structure, such as in $Au_{20}Cd_4(SH)(CHT)_{19}$ (CHT = S-*c*-C_6H_{11}).[9d] Last, the third case is that the Cd atoms substitute the staple Au atoms 1:2 without essentially changing the kernel structure, as in $[Au_{19}Cd_2(CHT)_{16}]$.[9b] However, it is unknown whether there are any other alloying modes and whether the Cd atom(s) can be removed (dealloyed) with the structure changed or not, especially whether the two-way alloying and dealloying of metalloid gold clusters can be achieved. Antigalvanic[8e,9a,c,d,10] and quasi-antigalvanic[9d,10a,11] reactions were recently introduced into nanochemistry for the synthesis of alloy or monometal clusters. Interestingly, we fullfilled the two-way alloying and dealloying of cadmium in metalloid gold clusters by successively employing the antigalvanic and quasi-antigalvanic methods.

$Au_{34}(CHT)_{22}$[12] was chosen as the precursor cluster because of its facile access to us. The Cd alloying of $Au_{34}(CHT)_{22}$ via an antigalvanic reaction is very facile. For reaction details, see the Supporting Information, and for UV−vis/near-IR (NIR) spectroscopy monitoring, see Figure S1. The formula of the as-prepared material was determined by electrospray ionization mass spectrometry (ESI-MS) in positive mode, assisted by cesium acetate (CsOAC). Note that no rational signals were obtained from both positive and negative ionization modes without the addition of CsOAC, which implies charge neutrality of the as-obtained clusters (Figure S2). Additional experimental results provide support for this (Figures S3 and S4). Figure 1 shows one dominant peak centered at m/z 4187.08 corresponding to the $[Au_{26}Cd_4(CHT)_{22} + 2Cs]^{2+}$ species (calcd, m/z 4186.93; deviation, m/z 0.15), and the calculated isotopic pattern is in agreement with the experimental isotopic pattern

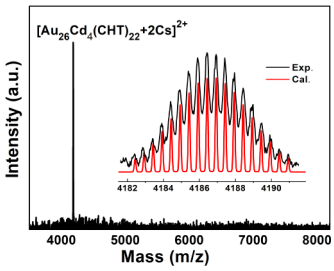

Figure 1. ESI-MS spectra of the as-prepared $Au_{26}Cd_4(CHT)_{22}$.

Received: January 14, 2019

DOI: 10.1021/acs.inorgchem.9b00125
Inorg. Chem. XXXX, XXX, XXX−XXX

(see the inset of Figure 1). Thereby the formula of the as-prepared cluster is concluded to be $Au_{26}Cd_4(CHT)_{22}$, which was further supported by X-ray photoelectron spectroscopy (XPS) and thermogravimetric analysis (TGA): XPS reveals a Au/Cd/S atomic ratio of 26/4.07/21.96, very close to the expected ratio of 26/4/22 for $Au_{26}Cd_4(CHT)_{22}$; TGA shows a weight loss of 31.08 wt %, in well agreement with the theoretical value (31.24 wt %; Figure S5) of $Au_{26}Cd_4(CHT)_{22}$.

The complete structure of the $Au_{26}Cd_4(CHT)_{22}$ cluster was revealed by X-ray crystallography (XRC), as shown in Figure S6. The absence of a counterion also provides evidence for neutrality of the as-obtained clusters. Parts a−c of Figure 2 depict structural details of $Au_{26}Cd_4(CHT)_{22}$, which contains a distorted face-centered-cubic (fcc) Au_{16} kernel capped by two "paw-like" $Cd(S{-}Au{-}S)_3$ motifs, one pentameric $Au_3Cd_2(SR)_8$ motif and one monomer $Au(SR)_2$ motif. The $Au_3Cd_2(SR)_8$ motif was not previously reported in metalloid clusters. It was revealed that the structural framework of $Au_{26}Cd_4(CHT)_{22}$ resembled that of $Au_{34}(CHT)_{22}$[12] (Figure 2d−f), and it can be concluded that the "paw-like" $Cd(S{-}Au{-}S)_3$ motif might have originated from one monomeric −S−Au−S− motif and one trimeric −S−Au−S−Au−S−Au−S− motif, with one Cd atom replacing two neighboring surface Au atoms (Figure 2g). Cd substitution also induces the original staple motifs (two monomeric −S−Au−S− motifs and one trimeric −S−Au−S−Au−S−Au−S− motif) to transform into a newly found pentameric $Au_3Cd_2(SR)_8$ motif (Figure 2g), in which the average S−Cd−S bond angle is slightly larger than that in the $Cd(S{-}Au{-}S)_3$ motif (∼109° vs ∼104°, respectively). Notably, in the $Cd(S{-}Au{-}S)_3$ and $Au_3Cd_2(SR)_8$ motifs, the Cd−S bond length (varying from 2.55 to 2.61 Å) shows an obvious difference from the Au−S bond length (from 2.17 to 2.46 Å), indicating that the covalent radius of Cd is larger, as found in many tables (for an example, see the previous work conducted by Pyykko and Atsumi[13]). The close $Au_{kernel}{-}Cd_{staple}$ distance ranging from 2.78 to 3.01 Å indicates that the Cd atoms in the staple have strong interaction with the Au atoms in the kernel. Additionally, the compacting of the staple motif and the shortening of the intraparticle H−H distances after the replacement of two Au atoms by one Cd atom were also observed (Figure S7). For the case of $[Au_{19}Cd_2(CHT)_{16}]^-$, four surface Au atoms of $[Au_{23}(CHT)_{16}]^-$ were replaced by two Cd atoms, with the kernel being unchanged.[9b] In $Au_{26}Cd_4(CHT)_{22}$, a distinct kernel change was observed compared with $Au_{34}(CHT)_{22}$ and is probably due to the relatively heavy substitution of Cd in $Au_{26}Cd_4(CHT)_{22}$ compared with the substitution in $[Au_{19}Cd_2(CHT)_{16}]^-$. As shown in Figure 2h, it is suggested that two Au atoms (orange) in the $Au_{34}(CHT)_{22}$ cluster were shifted along the arrow direction. Because certain Au−Au bonds in the kernel were stretched to fracture, a distorted fcc Au_{16} kernel structure was created. It is found that the average $Au_{kernel}{-}Au_{kernel}$ bond length of $Au_{26}Cd_4(CHT)_{22}$ (2.84 Å) is a little shorter than the average $Au_{kernel}{-}Au_{kernel}$ bond length of $Au_{34}(CHT)_{22}$ (2.90 Å). Therefore, the Cd atoms not only replaced the surface Au atoms by a 1:2 Cd/Au ratio but also led to structural changes in the kernel. Such an alloying mode was not previously reported and can be listed as the fourth alloying mode of Cd in metalloid gold clusters.

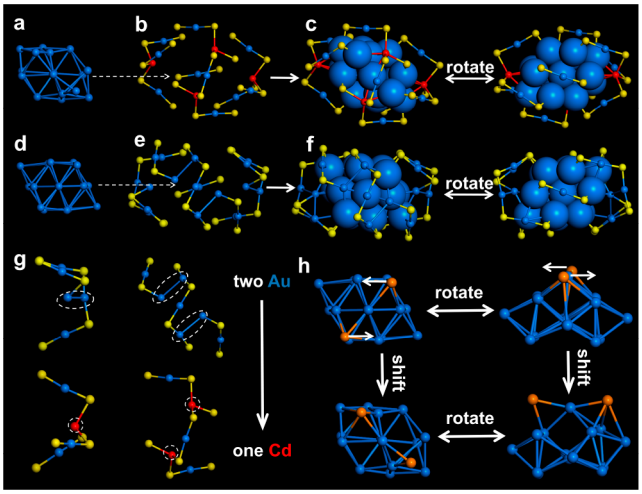

Figure 2. Structure of $Au_{26}Cd_4(CHT)_{22}$: kernel (a), surface motif (b), and the complete structure from different perspectives (c). Structure of $Au_{34}(CHT)_{22}$: kernel (d), surface motif (e), and the complete structure of from different perspectives (f). Comparison of the surface motifs $Au_{34}(CHT)_{22}$ (upper) and $Au_{26}Cd_4(CHT)_{22}$ (lower), in which one Cd atom replaces two nearby surface Au atoms (g). Comparison of the kernel structures $Au_{34}(CHT)_{22}$ (upper) and $Au_{26}Cd_4(CHT)_{22}$ (lower) (h). Color labels: yellow, S; red, Cd; others, Au. C and H atoms were omitted.

Interestingly, Cd alloying not only tailors the interior structure but also changes the exterior crystallographic arrangement from the 2H to 4H phase array (Figure 3). It was known that $[Au_{25-x}Ag_x(CHT)_{18}]^-$ ($x \sim 19$)[8f] and $Au_{20}Cd_4(SH)(CHT)_{19}$[9d] clusters also have different crystallographic arrangements compared with the parent $[Au_{23}(CHT)_{16}]^-$ clusters (Figure S8), which implies that alloying is also an effective way to influence the assembly of metalloid clusters.[14]

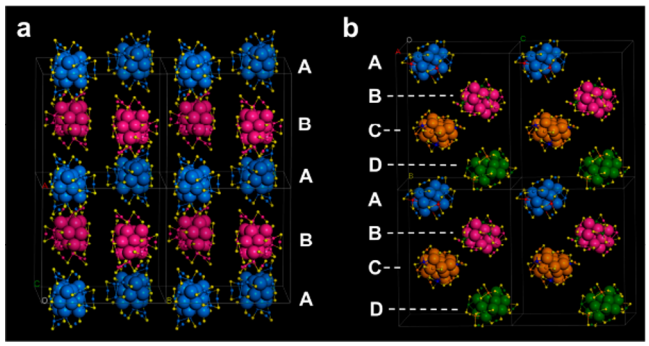

Figure 3. Crystallographic arrangement of the $Au_{34}(CHT)_{22}$ (a) and $Au_{26}Cd_4(CHT)_{22}$ (b) clusters in the single crystals. To highlight the arrangement, the Au and Cd atoms of the clusters in each close-packed plane are labeled in different colors.

Although the kernel of $Au_{26}Cd_4(CHT)_{22}$ is distorted, $Au_{26}Cd_4(CHT)_{22}$ shows higher thermostability than $Au_{34}(CHT)_{22}$ based on UV−vis/NIR (Figure S9) probably because of the formation of $Cd(SR)_3$ motifs. Note that some other influencing factors such as the protecting ligand and charge can be excluded and so can the nominal shell-closing electron count (N^*) because the two clusters have the same N^* ($N^*_{Au34} = N\nu A - M - z = 34 \times 1 - 22 - 0 = 12$; $N^*_{Au26Cd4} = 26 \times 1 + 4 \times 2 - 22 - 0 = 12$). Alloying not only strengthens the thermostability of the parent cluster but also effectively tunes the optical properties of the parent cluster, as supported by the maximum absorption shifts from 610 to 590 nm and from 465 to 479 nm, respectively (Figure S9). Besides, the maximum emission blue shifts from 807 to 763 nm, and the fluorescence

DOI: 10.1021/acs.inorgchem.9b00125
Inorg. Chem. XXXX, XXX, XXX−XXX

intensity decreases by approximately 48% (Figure S10). The emission blueshift may relate to the blueshift of the maximum absorption of the $Au_{34}(CHT)_{22}$ cluster in the NIR region, and the fluorescence intensity decrease may be attributed to the fact that the Cd atom has a weaker electron affinity than Au, thus inhibiting charge transfer from the ligand to the metal core through the metal−S bond.[15]

Reversible dealloying of Cd in $Au_{26}Cd_4(CHT)_{22}$ by a quasi-antigalvanic reaction[9d,10a,11] between $Au_{26}Cd_4(CHT)_{22}$ and the Au-CHT complex was observed (see Figures 4 and S11a and the Experimental Section). Mass spectrometry identified the product as $Au_{34}(CHT)_{22}$ (Figure S11b). Note that the reduction of Au^I is evidenced by the XPS results (Figure S12) and so is the reduction of Cd^{II} in the reaction between $Au_{34}(CHT)_{22}$ and Cd^{II} (Figure S13). Because the major metal in $Au_{26}Cd_4(CHT)_{22}$ is gold, the reaction between $Au_{26}Cd_4(CHT)_{22}$ and Au-CHT is named the quasi-antigalvanic reaction.[9d,10a,11] The redox reactions are also validated by cyclic voltammetry measurements (Figure S14). More interestingly, when the Au^I-CHT complex was replaced by a $Pt(CHT)_2$ complex (see Supporting Information for the reaction details), another dealloyed cluster, $Au_{18}(CHT)_{14}$,[16] with an entirely different structure was obtained (see Figure 4, and for the composition identification and Pt exclusion, see Figure S15). This finding indicates that the dealloying process is reactant-ion-dependent, which not only is interesting but also provides versatile tuning of the metal nanoparticles.

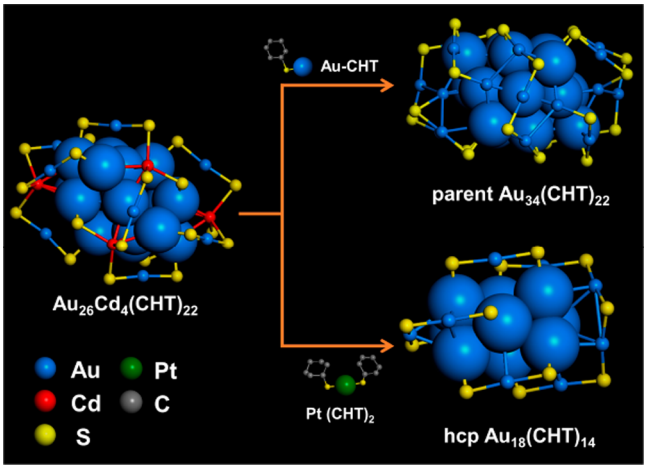

Figure 4. Au-CHT complex that induced the transformation of $Au_{26}Cd_4(CHT)_{22}$ to $Au_{34}(CHT)_{22}$ and $Pt(CHT)_2$ complex that induced the transformation of $Au_{26}Cd_4(CHT)_{22}$ to $Au_{18}(CHT)_{14}$. Color labels: yellow, S; red, Cd; others, Au; green, Pt; gray, C. H atoms were omitted.

In summary, we synthesized a novel Cd-alloyed metalloid gold cluster and precisely characterized it mainly with ESI-MS and XRC, which revealed a new Cd-alloying mode: Cd atoms occupy the parent cluster and change the kernel structure, resulting in the formation of a novel staple structure, $Au_3Cd_2(SR)_8$. The alloying not only influences the interior structure but also alters the exterior crystallographic arrangement from the 2H to 4H phase array. Cd alloying effectively tunes the stability and optical properties of the parent cluster. Interestingly, it was found that the as-obtained Cd-alloyed metalloid gold clusters can be dealloyed by a quasi-antigalvanic reaction with the structure changed or unchanged and that dealloying is a reactant-ion-dependent process. Overall, our work provides novel insight into the structure of Cd-alloyed metalloid gold clusters, has important implications toward the structure−property correlation, reveals novel chemistry of alloying and dealloying, and indicates a novel application of AGR. Therefore, it is expected that this work will open new avenues for engineering nanoparticles with atomic precision and stimulating more research on metal nanoparticle alloying and dealloying, as well as the structure−property correlation.

■ ASSOCIATED CONTENT

Supporting Information

The Supporting Information is available free of charge on the ACS Publications website at DOI: 10.1021/acs.inorgchem.9b00125.

Detailed synthesis method, characterization, crystal structure refinements, Figures S1−S15, and Table S1 (PDF)

Accession Codes

CCDC 1871814 contains the supplementary crystallographic data for this paper. These data can be obtained free of charge via www.ccdc.cam.ac.uk/data_request/cif, or by emailing data_request@ccdc.cam.ac.uk, or by contacting The Cambridge Crystallographic Data Centre, 12 Union Road, Cambridge CB2 1EZ, UK; fax: +44 1223 336033.

■ AUTHOR INFORMATION

Corresponding Author

*E-mail: zkwu@issp.ac.cn.

ORCID

Haiteng Deng: 0000-0003-2753-4590

Zhikun Wu: 0000-0002-2711-3860

Author Contributions

⊥W.Z. and S.Z. contributed equally.

Notes

The authors declare no competing financial interest.

■ ACKNOWLEDGMENTS

The authors thank the Natural Science Foundation of China (Grants 21222301, 21771186, 21829501, 21603234, 21701179, 21171170, and 21528303), the Key Program of the 13th five-year plan, CASHIPS (KP-2017-16), the CASHIPS Director's Fund (BJPY2019A02), the CAS/SAFEA International Partnership Program for Creative Research Teams, and the Innovative Program of the Development Foundation of Hefei Center for Physical Science and Technology (Grant 2017FXCX002) for financial support.

■ REFERENCES

(1) (a) Ferrando, R.; Jellinek, J.; Johnston, R. L. Nanoalloys: From Theory to Applications of Alloy Clusters and Nanoparticles. *Chem. Rev.* **2008**, *108*, 845−910. (b) Yuan, X.; Dou, X.; Zheng, K.; Xie, J. Recent Advances in the Synthesis and Applications of Ultrasmall Bimetallic Nanoclusters. *Part. Part. Syst. Charact.* **2015**, *32*, 613−629. (c) Kwak, K.; Choi, W.; Tang, Q.; Kim, M.; Lee, Y.; Jiang, D. E.; Lee, D. A molecule-like $PtAu_{24}(SC_6H_{13})_{18}$ nanocluster as an electrocatalyst for hydrogen production. *Nat. Commun.* **2017**, *8*, 14723. (d) Chen, G.; Zhao, Y.; Fu, G.; Duchesne, P. N.; Gu, L.; Zheng, Y.; Weng, X.; Chen, M.; Zhang, P.; Pao, C.-W.; Lee, J.-F.; Zheng, N. Interfacial Effects in Iron-Nickel Hydroxide-Platinum Nanoparticles Enhance Catalytic Oxidation. *Science* **2014**, *344*, 495−499. (e) Huang, X.; Zhao, Z.; Cao, L.; Chen, Y.; Zhu, E.; Lin, Z.; Li, M.; Yan, A.; Zettl, A.; Wang, Y. M.; Duan, X.; Mueller, T.; Huang, Y. High-performance transition

DOI: 10.1021/acs.inorgchem.9b00125
Inorg. Chem. XXXX, XXX, XXX−XXX

metal-doped Pt_3Ni octahedra for oxygen reduction reaction. *Science* **2015**, *348*, 1230−1234.

(2) Jin, R.; Zeng, C.; Zhou, M.; Chen, Y. Atomically Precise Colloidal Metal Nanoclusters and Nanoparticles: Fundamentals and Opportunities. *Chem. Rev.* **2016**, *116*, 10346−10413.

(3) (a) Schnepf, A.; Schnöckel, H. Metalloid Aluminum and Gallium Clusters: Element Modifications on the Molecular Scale? *Angew. Chem., Int. Ed.* **2002**, *41*, 3532−3552. (b) Schnöckel, H. Structures and Properties of Metalloid Al and Ga Clusters Open Our Eyes to the Diversity and Complexity of Fundamental Chemical and Physical Processes during Formation and Dissolution of Metal. *Chem. Rev.* **2010**, *110*, 4125−4163. (c) Lu, Y.; Chen, W. Sub-nanometre sized metal clusters: from synthetic challenges to the unique property discoveries. *Chem. Soc. Rev.* **2012**, *41*, 3594−3623. (d) Knoppe, S.; Burgi, T. Chirality in Thiolate-Protected Gold Clusters. *Acc. Chem. Res.* **2014**, *47*, 1318−1326. (e) Yamazoe, S.; Koyasu, K.; Tsukuda, T. Nonscalable Oxidation Catalysis of Gold Clusters. *Acc. Chem. Res.* **2014**, *47*, 816−824. (f) Chakraborty, I.; Pradeep, T. Atomically Precise Clusters of Noble Metals: Emerging Link between Atoms and Nanoparticles. *Chem. Rev.* **2017**, *117*, 8208−8271. (g) Mayer, K.; Wessing, J.; Fässler, T. F.; Fischer, R. A. Intermetalloid Clusters: Molecules and Solids in a Dialogue. *Angew. Chem., Int. Ed.* **2018**, *57*, 14372−14393.

(4) (a) Brust, M.; Walker, M.; Bethell, D.; Schiffrin, D. J.; Whyman, R. Synthesis of Thiol-derivatised Gold Nanoparticles in a Two-phase Liquid-Liquid System. *J. Chem. Soc., Chem. Commun.* **1994**, *7*, 801−802. (b) Wu, Z.; Suhan, J.; Jin, R. One-pot synthesis of atomically monodisperse, thiol-functionalized Au_{25} nanoclusters. *J. Mater. Chem.* **2009**, *19*, 622−626. (c) Wu, Z.; MacDonald, M. A.; Chen, J.; Zhang, P.; Jin, R. Kinetic Control and Thermodynamic Selection in the Synthesis of Atomically Precise Gold Nanoclusters. *J. Am. Chem. Soc.* **2011**, *133*, 9670−9673.

(5) (a) Jadzinsky, P. D.; Calero, G.; Ackerson, C. J.; Bushnell, D. A.; Kornberg, R. D. Structure of a Thiol Monolayer-Protected Gold Nanoparticle at 1.1 Å resolution. *Science* **2007**, *318*, 430−433. (b) Heaven, M. W.; Dass, A.; White, P. S.; Holt, K. M.; Murray, R. W. Crystal Structure of the Gold Nanoparticle $[N(C_8H_{17})_4]$-$[Au_{25}(SCH_2CH_2Ph)_{18}]$. *J. Am. Chem. Soc.* **2008**, *130*, 3754−3755. (c) Zhu, M.; Aikens, C. M.; Hollander, F. J.; Schatz, G. C.; Jin, R. Correlating the Crystal Structure of A Thiol-Protected Au_{25} Cluster and Optical Properties. *J. Am. Chem. Soc.* **2008**, *130*, 5883−5885. (d) Liu, C.; Li, T.; Li, G.; Nobusada, K.; Zeng, C.; Pang, G.; Rosi, N. L.; Jin, R. Observation of Body-Centered Cubic Gold Nanocluster. *Angew. Chem., Int. Ed.* **2015**, *54*, 9826−9829. (e) Liao, L.; Zhuang, S.; Wang, P.; Xu, Y.; Yan, N.; Dong, H.; Wang, C.; Zhao, Y.; Xia, N.; Li, J.; Deng, H.; Pei, Y.; Tian, S. K.; Wu, Z. Quasi-Dual-Packed-Kerneled Au_{49}(2, 4-DMBT)$_{27}$ Nanoclusters and the Influence of Kernel Packing on the Electrochemical Gap. *Angew. Chem., Int. Ed.* **2017**, *56*, 12644−12648.

(6) (a) Wu, Z.; Wang, M.; Yang, J.; Zheng, X.; Cai, W.; Meng, G.; Qian, H.; Wang, H.; Jin, R. Well-Defined Nanoclusters as Fluorescent Nanosensors: A Case Study on $Au_{25}(SG)_{18}$. *Small* **2012**, *8*, 2028−2035. (b) Antonello, S.; Perera, N. V.; Ruzzi, M.; Gascon, J. A.; Maran, F. Interplay of Charge State, Lability, and Magnetism in the Molecule-like $Au_{25}(SR)_{18}$ cluster. *J. Am. Chem. Soc.* **2013**, *135*, 15585−15594. (c) Chen, Y. S.; Choi, H.; Kamat, P. V. Metal-Cluster-Sensitized Solar Cells. A New Class of Thiolated Gold Sensitizers Delivering Efficiency Greater Than 2%. *J. Am. Chem. Soc.* **2013**, *135*, 8822−8825. (d) Yi, C.; Tofanelli, M. A.; Ackerson, C. J.; Knappenberger, K. L., Jr. Optical Properties and Electronic Energy Relaxation of Metallic $Au_{144}(SR)_{60}$ Nanoclusters. *J. Am. Chem. Soc.* **2013**, *135*, 18222−18228. (e) Knoppe, S.; Wong, O. A.; Malola, S.; Hakkinen, H.; Burgi, T.; Verbiest, T.; Ackerson, C. J. Chiral Phase Transfer and Enantioenrichment of Thiolate-Protected Au_{102} Clusters. *J. Am. Chem. Soc.* **2014**, *136*, 4129−4132. (f) Zhang, X. D.; Luo, Z.; Chen, J.; Shen, X.; Song, S.; Sun, Y.; Fan, S.; Fan, F.; Leong, D. T.; Xie, J. Ultrasmall $Au_{10-12}(SG)_{10-12}$ Nanomolecules for High Tumor Specificity and Cancer Radiotherapy. *Adv. Mater.* **2014**, *26*, 4565−4568. (g) Du, B.; Jiang, X.; Das, A.; Zhou, Q.; Yu, M.; Jin, R.; Zheng, J. Glomerular barrier behaves as an atomically precise bandpass filter in a sub-nanometre regime. *Nat. Nanotechnol.* **2017**, *12*, 1096−1102.

(7) (a) Desireddy, A.; Conn, B. E.; Guo, J.; Yoon, B.; Barnett, R. N.; Monahan, B. M.; Kirschbaum, K.; Griffith, W. P.; Whetten, R. L.; Landman, U.; Bigioni, T. P. Ultrastable silver nanoparticles. *Nature* **2013**, *501*, 399−402. (b) Dhayal, R. S.; Liao, J. H.; Liu, Y. C.; Chiang, M. H.; Kahlal, S.; Saillard, J. Y.; Liu, C. W. $[Ag_{21}\{S_2P(OiPr)_2\}_{12}]^+$: An Eight-Electron Superatom. *Angew. Chem., Int. Ed.* **2015**, *54*, 3702−3706. (c) Negishi, Y.; Nakazaki, T.; Malola, S.; Takano, S.; Niihori, Y.; Kurashige, W.; Yamazoe, S.; Tsukuda, T.; Hakkinen, H. A Critical Size for Emergence of Nonbulk Electronic and Geometric Structures in Dodecanethiolate-Protected Au Clusters. *J. Am. Chem. Soc.* **2015**, *137*, 1206−1212. (d) Tian, S.; Li, Y. Z.; Li, M. B.; Yuan, J.; Yang, J.; Wu, Z.; Jin, R. Structural isomerism in gold nanoparticles revealed by X-ray crystallography. *Nat. Commun.* **2015**, *6*, 8667. (e) Alhilaly, M. J.; Bootharaju, M. S.; Joshi, C. P.; Besong, T. M.; Emwas, A. H.; Juarez-Mosqueda, R.; Kaappa, S.; Malola, S.; Adil, K.; Shkurenko, A.; Hakkinen, H.; Eddaoudi, M.; Bakr, O. M. $[Ag_{67}(SPhMe_2)_{32}(PPh_3)_8]^{3+}$: Synthesis, Total Structure, and Optical Properties of a Large Box-Shaped Silver Nanocluster. *J. Am. Chem. Soc.* **2016**, *138*, 14727−14732. (f) Yang, H.; Wang, Y.; Chen, X.; Zhao, X.; Gu, L.; Huang, H.; Yan, J.; Xu, C.; Li, G.; Wu, J.; Edwards, A. J.; Dittrich, B.; Tang, Z.; Wang, D.; Lehtovaara, L.; Hakkinen, H.; Zheng, N. Plasmonic twinned silver nanoparticles with molecular precision. *Nat. Commun.* **2016**, *7*, 12809. (g) Zeng, C.; Chen, Y.; Kirschbaum, K.; Lambright, K. J.; Jin, R. Emergence of hierarchical structural complexities in nanoparticles and their assembly. *Science* **2016**, *354*, 1580−1584. (h) Gan, Z.; Chen, J.; Wang, J.; Wang, C.; Li, M. B.; Yao, C.; Zhuang, S.; Xu, A.; Li, L.; Wu, Z. The fourth crystallographic closest packing unveiled in the gold nanocluster crystal. *Nat. Commun.* **2017**, *8*, 14739. (i) Kenzler, S.; Schrenk, C.; Schnepf, A. $Au_{108}S_{24}(PPh_3)_{16}$: A Highly Symmetric Nanoscale Gold Cluster Confirms the General Concept of Metalloid Clusters. *Angew. Chem., Int. Ed.* **2017**, *56*, 393−396. (j) Sakthivel, N. A.; Theivendran, S.; Ganeshraj, V.; Oliver, A. G.; Dass, A. Crystal Structure of Faradaurate-279: Au_{279}(SPh-*t*Bu)$_{84}$ Plasmonic Nanocrystal Molecules. *J. Am. Chem. Soc.* **2017**, *139*, 15450−15459. (k) He, L.; Yuan, J.; Xia, N.; Liao, L.; Liu, X.; Gan, Z.; Wang, C.; Yang, J.; Wu, Z. Kernel Tuning and Nonuniform Influence on Optical and Electrochemical Gaps of Bimetal Nanoclusters. *J. Am. Chem. Soc.* **2018**, *140*, 3487−3490. (l) Huang, R. W.; Dong, X. Y.; Yan, B. J.; Du, X. S.; Wei, D. H.; Zang, S. Q.; Mak, T. C. W. Tandem Silver Cluster Isomerism and Mixed Linkers to Modulate the Photoluminescence of Cluster-Assembled Materials. *Angew. Chem., Int. Ed.* **2018**, *57*, 8560−8566. (m) Kurasawa, M.; Arisaka, F.; Ozeki, T. Asymmetricallyfused polyoxometalate-silver alkynide composite cluster. *Inorg. Chem.* **2015**, *54*, 1650−1654. (n) Chen, J.; Zhang, Q.-F.; Williard, P. G.; Wang, L.-S. Synthesis and Structure Determination of a New Au_{20} Nanocluster Protected by Tripodal Tetraphosphine Ligands. *Inorg. Chem.* **2014**, *53*, 3932−3934. (o) Sheong, F. K.; Zhang, J. X.; Lin, Z. An $[Au_{13}]^{5+}$ Approach to the Study of Gold Nanoclusters. *Inorg. Chem.* **2016**, *55*, 11348−11353. (p) Nguyen, T.-A. D.; Cook, A. W.; Wu, G.; Hayton, T. W. Subnanometer-Sized Copper Clusters: A Critical Re-evaluation of the Synthesis and Characterization of $Cu_8(MPP)_4$ (HMPP = 2-Mercapto-5-n-propylpyrimidine). *Inorg. Chem.* **2017**, *56*, 8390−8396. (q) Liu, J. W.; Feng, L.; Su, H. F.; Wang, Z.; Zhao, Q. Q.; Wang, X. P.; Tung, C. H.; Sun, D.; Zheng, L. S. Anisotropic Assembly of Ag_{52} and Ag_{76} Nanoclusters. *J. Am. Chem. Soc.* **2018**, *140*, 1600−1603. (r) Yan, B. J.; Du, X. S.; Huang, R. W.; Yang, J. S.; Wang, Z. Y.; Zang, S. Q.; Mak, T. C. W. Self-Assembly of a Stable Silver Thiolate Nanocluster Encapsulating a Lacunary Keggin Phosphotungstate Anion. *Inorg. Chem.* **2018**, *57*, 4828−4832. (s) Takano, S.; Hirai, H.; Muramatsu, S.; Tsukuda, T. Hydride-Doped Gold Superatom $(Au_9H)^{2+}$: Synthesis, Structure, and Transformation. *J. Am. Chem. Soc.* **2018**, *140*, 8380−8383. (t) Huber, M.; Schnepf, A.; Anson, C. E.; Schnöckel, H. Si@Al_{56} $[N(2, 6\text{-}iPr_2C_6H_3)SiMe_3]_{12}$: The Largest Neutral Metalloid Aluminum Cluster, a Molecular Model for a Silicon-Poor Aluminum-Silicon Alloy? *Angew. Chem., Int. Ed.* **2008**, *47*, 8201−8206. (u) Weinert, B.; Muller, F.; Harms, K.; Clerac, R.; Dehnen, S. Origin and Location of Electrons and Protons during the Formation of Intermetalloid Clusters $[Sm@Ga_{3-x}H_{3-2x}Bi_{10+x}]^{3-}$ (x = 0, 1). *Angew. Chem., Int. Ed.* **2014**, *53*, 11979−11983.

DOI: 10.1021/acs.inorgchem.9b00125
Inorg. Chem. XXXX, XXX, XXX−XXX

(8) (a) Gao, Y.; Shao, N.; Pei, Y.; Zeng, X. C. Icosahedral Crown Gold Nanocluster $Au_{43}Cu_{12}$ with High Catalytic Activity. *Nano Lett.* **2010**, *10*, 1055−1062. (b) Yang, H.; Wang, Y.; Huang, H.; Gell, L.; Lehtovaara, L.; Malola, S.; Häkkinen, H.; Zheng, N. All-thiol-stabilized Ag_{44} and $Au_{12}Ag_{32}$ nanoparticles with single-crystal structures. *Nat. Commun.* **2013**, *4*, 2422. (c) Kumara, C.; Aikens, C. M.; Dass, A. X-ray Crystal Structure and Theoretical Analysis of $Au_{25-x}Ag_x(SCH_2CH_2Ph)_{18}^-$ Alloy. *J. Phys. Chem. Lett.* **2014**, *5*, 461−466. (d) Wang, S.; Jin, S.; Yang, S.; Chen, S.; Song, Y.; Zhang, J.; Zhu, M. Total structure determination of surface doping $[Ag_{46}Au_{24}(SR)_{32}]$-$(BPh_4)_2$ nanocluster and its structure-related catalytic property. *Sci. Adv.* **2015**, *1*, No. e1500441. (e) Yao, C.; Chen, J.; Li, M.-B.; Liu, L.; Yang, J.; Wu, Z. Adding Two Active Silver Atoms on Au_{25} Nanoparticle. *Nano Lett.* **2015**, *15*, 1281−1287. (f) Li, Q.; Wang, S.; Kirschbaum, K.; Lambright, K. J.; Das, A.; Jin, R. Heavily doped $Au_{25-x}Ag_x(SC_6H_{11})_{18}^-$ nanoclusters: silver goes from the core to the surface. *Chem. Commun.* **2016**, *52*, 5194−5197. (g) Bootharaju, M. S.; Joshi, C. P.; Parida, M. R.; Mohammed, O. F.; Bakr, O. M. Templated Atom-Precise Galvanic Synthesis and Structure Elucidation of a $[Ag_{24}Au(SR)_{18}]^-$ Nanocluster. *Angew. Chem., Int. Ed.* **2016**, *55*, 922−926. (h) Zeng, J. L.; Guan, Z. J.; Du, Y.; Nan, Z. A.; Lin, Y. M.; Wang, Q. M. Chloride-Promoted Formation of a Bimetallic Nanocluster $Au_{80}Ag_{30}$ and the Total Structure Determination. *J. Am. Chem. Soc.* **2016**, *138*, 7848−7851. (i) Li, Q.; Luo, T.-Y.; Taylor, M. G.; Wang, S.; Zhu, X.; Song, Y.; Mpourmpakis, G.; Rosi, N. L.; Jin, R. Molecular "surgery" on a 23-gold-atom nanoparticle. *Sci. Adv.* **2017**, *3*, No. e1603193. (j) Wan, X. K.; Cheng, X. L.; Tang, Q.; Han, Y. Z.; Hu, G.; Jiang, D. E.; Wang, Q. M. Atomically Precise Bimetallic $Au_{19}Cu_{30}$ Nanocluster with an Icosidodecahedral Cu_{30} Shell and an Alkynyl-Cu Interface. *J. Am. Chem. Soc.* **2017**, *139*, 9451−9454. (k) Yao, Q.; Feng, Y.; Fung, V.; Yu, Y.; Jiang, D. E.; Yang, J.; Xie, J. Precise control of alloying sites of bimetallic nanoclusters via surface motif exchange reaction. *Nat. Commun.* **2017**, *8*, 1555. (l) Deng, G.; Malola, S.; Yan, J.; Han, Y.; Yuan, P.; Zhao, C.; Yuan, X.; Lin, S.; Tang, Z.; Teo, B. K.; Hakkinen, H.; Zheng, N. From Symmetry Breaking to Unraveling the Origin of the Chirality of Ligated $Au_{13}Cu_2$ Nanoclusters. *Angew. Chem., Int. Ed.* **2018**, *57*, 3421−3425. (m) Jin, S.; Xu, F.; Du, W.; Kang, X.; Chen, S.; Zhang, J.; Li, X.; Hu, D.; Wang, S.; Zhu, M. Isomerism in Au-Ag Alloy Nanoclusters: Structure Determination and Enantioseparation of $[Au_9Ag_{12}(SR)_4(dppm)_6X_6]^{3+}$. *Inorg. Chem.* **2018**, *57*, 5114−5119.

(9) (a) Liao, L.; Zhou, S.; Dai, Y.; Liu, L.; Yao, C.; Fu, C.; Yang, J.; Wu, Z. Mono-Mercury Doping of Au_{25} and the HOMO/LUMO Energies Evaluation Employing Differential Pulse Voltammetry. *J. Am. Chem. Soc.* **2015**, *137*, 9511−9514. (b) Li, Q.; Lambright, K. J.; Taylor, M. G.; Kirschbaum, K.; Luo, T. Y.; Zhao, J.; Mpourmpakis, G.; Mokashi-Punekar, S.; Rosi, N. L.; Jin, R. Reconstructing the Surface of Gold Nanoclusters by Cadmium Doping. *J. Am. Chem. Soc.* **2017**, *139*, 17779−17782. (c) Yao, C.; Lin, Y.-j.; Yuan, J.; Liao, L.; Zhu, M.; Weng, L.-h.; Yang, J.; Wu, Z. Mono-cadmium vs Mono-mercury Doping of Au_{25} Nanoclusters. *J. Am. Chem. Soc.* **2015**, *137*, 15350−15353. (d) Zhu, M.; Wang, P.; Yan, N.; Chai, X.; He, L.; Zhao, Y.; Xia, N.; Yao, C.; Li, J.; Deng, H.; Zhu, Y.; Pei, Y.; Wu, Z. The Fourth Alloying Mode by Way of Anti-Galvanic Reaction. *Angew. Chem., Int. Ed.* **2018**, *57*, 4500−4504. (e) Yang, S.; Chen, S.; Xiong, L.; Liu, C.; Yu, H.; Wang, S.; Rosi, N. L.; Pei, Y.; Zhu, M. Total Structure Determination of Au_{16}(S-Adm)$_{12}$ and $Cd_1Au_{14}(StBu)_{12}$ and Implications for the Structure of $Au_{15}(SR)_{13}$. *J. Am. Chem. Soc.* **2018**, *140*, 10988−10994.

(10) (a) Gan, Z.; Xia, N.; Wu, Z. Discovery, Mechanism, and Application of Antigalvanic Reaction. *Acc. Chem. Res.* **2018**, *51*, 2774−2783. (b) Wu, Z. Anti-Galvanic Reduction of Thiolate-Protected Gold and Silver Nanoparticles. *Angew. Chem., Int. Ed.* **2012**, *51*, 2934−2938. (c) Wang, M.; Wu, Z.; Chu, Z.; Yang, J.; Yao, C. Chemico-Physical Synthesis of Surfactant- and Ligand-Free Gold Nanoparticles and Their Anti-Galvanic Reduction Property. *Chem. - Asian J.* **2014**, *9*, 1006−1010. (d) Li, M. B.; Tian, S. K.; Wu, Z.; Jin, R. Cu^{2+} induced formation of $Au_{44}(SC_2H_4Ph)_{32}$ and its high catalytic activity for the reduction of 4-nitrophenol at low temperature. *Chem. Commun.* **2015**, *51*, 4433−4436. (e) Tian, S.; Yao, C.; Liao, L.; Xia, N.; Wu, Z. Ion-precursor and ion-dose dependent anti-galvanic reduction. *Chem. Commun.* **2015**, *51*, 11773−11776. (f) Li, M.-B.; Tian, S.-K.; Wu, Z. Improving the Catalytic Activity of Au_{25} Nanocluster by Peeling and Doping. *Chin. J. Chem.* **2017**, *35*, 567−571. (g) Liu, X.; Astruc, D. From Galvanic to Anti-Galvanic Synthesis of Bimetallic Nanoparticles and Applications in Catalysis, Sensing, and Materials Science. *Adv. Mater.* **2017**, *29*, 1605305.

(11) Yao, C.; Tian, S.; Liao, L.; Liu, X.; Xia, N.; Yan, N.; Gan, Z.; Wu, Z. Synthesis of fluorescent phenylethanethiolated gold nanoclusters via pseudo-AGR method. *Nanoscale* **2015**, *7*, 16200−16203.

(12) Dong, H.; Liao, L.; Zhuang, S.; Yao, C.; Chen, J.; Tian, S.; Zhu, M.; Liu, X.; Li, L.; Wu, Z. A novel double-helical-kernel evolution pattern of gold nanoclusters: alternate single-stranded growth at both ends. *Nanoscale* **2017**, *9*, 3742−3746.

(13) Pyykko, P.; Atsumi, M. Molecular Single-Bond Covalent Radii for Elements 1−118. *Chem. - Eur. J.* **2009**, *15*, 186−197.

(14) (a) Nag, A.; Chakraborty, P.; Bodiuzzaman, M.; Ahuja, T.; Antharjanam, S.; Pradeep, T. Polymorphism of $Ag_{29}(BDT)_{12}(TPP)_4^{3-}$ cluster: interactions of secondary ligands and their effect on solid state luminescence. *Nanoscale* **2018**, *10*, 9851−9855. (b) Gan, Z.; Chen, J.; Liao, L.; Zhang, H.; Wu, Z. Surface Single-Atom Tailoring of a Gold Nanoparticle. *J. Phys. Chem. Lett.* **2018**, *9*, 204−208.

(15) Liu, X.; Yuan, J.; Yao, C.; Chen, J.; Li, L.; Bao, X.; Yang, J.; Wu, Z. Crystal and Solution Photoluminescence of $MAg_{24}(SR)_{18}$ (M = Ag/Pd/Pt/Au) Nanoclusters and Some Implications for the Photoluminescence Mechanisms. *J. Phys. Chem. C* **2017**, *121*, 13848−13853.

(16) Das, A.; Liu, C.; Byun, H. Y.; Nobusada, K.; Zhao, S.; Rosi, N.; Jin, R. Structure Determination of $[Au_{18}(SR)_{14}]$. *Angew. Chem., Int. Ed.* **2015**, *54*, 3140−3144.

DOI: 10.1021/acs.inorgchem.9b00125
Inorg. Chem. XXXX, XXX, XXX−XXX